RULING FACTORS IN THE IMPACT OF COLLISION DEBRIS ON THE LHC HIGH LUMINOSITY INSERTION MAGNETS

A. Mereghetti, F. Cerutti, A. Ferrari, E. Todesco, E. Wildner
CERN, Geneva, Switzerland

Email contact of main author: alessio.mereghetti@cern.ch

Abstract. The Large Hadron Collider (LHC) built at CERN now enters a starting-up phase in order to reach the present design luminosity (L_0) of 10^{34} cm$^{-2}\cdot$s^{-1}. A possible upgrade of the machine to a luminosity value of 10 L_0 requires a new design of some insertion region magnets, and will be implemented in essentially two phases. The energy from collision debris is deposited in the insertion region magnetic elements and in particular in the superconducting magnet coils with a possible risk of quench. The role of the key parameters (such as the magnet aperture, the crossing plane, the thickness of a possible shielding liner, …) is pointed out, in order to optimize the design of the new insertion regions for the Upgrade phase I aiming to reach 2–3 L_0.

1. Introduction

The Large Hadron Collider (LHC) built at CERN now enters a starting-up phase in order to reach the present design luminosity (L_0) of 10^{34} cm$^{-2}\cdot$s^{-1}. A two-stage upgrade of the machine is envisaged in order to increase the luminosity by one order of magnitude: the goal of the Phase I Upgrade is to reach 2-3 L_0, whereas the following Phase II Upgrade shall bring the luminosity up to the ultimate value of 10 L_0.

The actual layout of the machine on both sides of the high luminosity experiments ATLAS and CMS at Point 1 and 5, respectively, consists of a sequence of three quadrupoles (the 'triplet', provided with corrector magnets) followed by a couple of separation dipoles ('D1' and 'D2' in FIG. 1.) [1]. The role of the triplet is to squeeze the beam in the interaction point (IP) down to β*=0.55 m. The luminosity upgrade relies in part on increasing the beam current, and mostly on increasing the triplet focusing, lowering the value of β* from the nominal value down to 0.3 m, or less if possible. The actual triplet aperture of 70 mm does not allow a further squeeze since the beam would become too large in the triplet itself. Consequently, the Phase I Upgrade foresees to re-design the triplet with its correctors and one of the two separation dipoles.
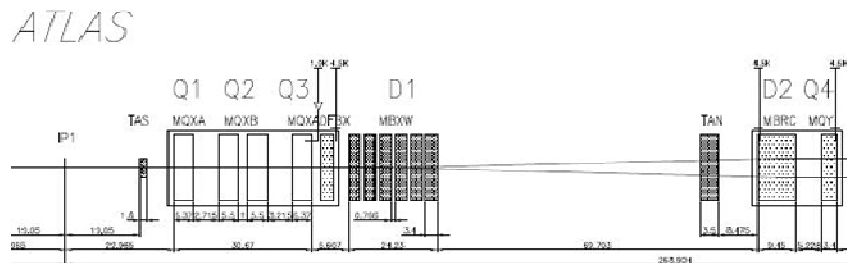

FIG. 1. Actual layout of the beam line on one side of the ATLAS experiment.

The new triplet [2] will employ the technology of Nb-Ti Rutherford-type cables cooled at 1.9 K already developed for the LHC main dipoles on a two-layered design. It will feature an aperture of 120 mm and will be longer than the present one (see FIG. 2.). An increased Beam Screen (BS) thickness is envisaged only for the Q1 (see Section 3.1). The corrector magnets will be grouped

in one package at the non-IP side of the triplet (a possible corrector dipole in-between the triplet elements is currently under consideration), followed by a superconducting, RHIC-style separation dipole, provided with a large aperture (180 mm).
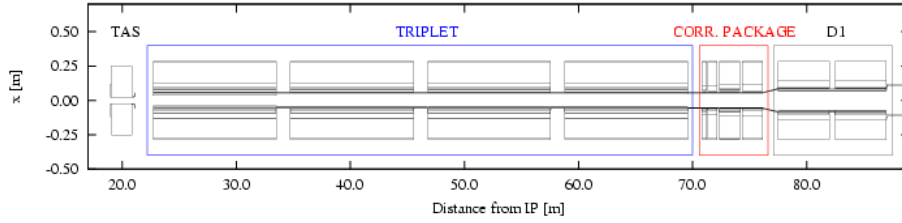

FIG. 2. Layout of the insertion region magnets used for the energy deposition studies for the Phase I Upgrade.

The debris due to proton-proton collisions causes a continuous heat load in the superconducting coils, especially in the triplet: a proper protection of the magnets should be envisaged to prevent their quench. For the present LHC triplets the coil protection has been achieved within a safety factor of three with respect to the estimated quench limit, for the nominal luminosity L_0 [3]. As the power density from the debris scales with luminosity, a higher protection efficiency is required than in the actual triplet. For the purposes of the new triplet conceptual design [4], the same heat transfer properties as in the actual one are assumed, i.e. the same cooling capacity is available and a maximum power density of $4.3 \text{ mW} \cdot \text{cm}^{-3}$ in the coils is taken as the design limit.

The Monte Carlo code FLUKA [5,6] was used for energy deposition studies, provided with the event generator DPMJET [7] for the description of the primary proton-proton interactions at 14 TeV centre-of-mass energy. Results are generally affected by 10% statistical uncertainties on peak values, whereas a 1% statistical uncertainty is usually achieved on the totals. Systematic uncertainties related to the extrapolation of the cross sections for the primary events, interaction/transport models, geometry and material implementation, crucial dependence on a very small angular range of the reaction products are unavoidable, and a safety margin of a factor of three for the peak power density is a necessary assumption for this kind of calculations.

2.   Characterization of the collision debris

The interface between the LHC machine and the high luminosity Insertion Regions (IR) is the Target Absorber of Secondaries (TAS), the goal of which is to protect the first magnetic elements of the machine from the collision debris and to reduce backscattered radiation to the experiment detector. Nevertheless, 10% of the total number[1] of particles generated in the proton-proton collisions goes through the TAS aperture, carrying almost 80% of the energy, mainly shared among protons, neutrons, charged hadrons and photons.

FIG. 3. shows the spectra of different particle families inside the vacuum chamber at the non-IP side of the TAS and of each triplet element. Charged particles (especially pions) are captured by the triplet magnetic field, leading to showering outside the aperture limit represented by the BS. This effect is responsible for the strong attenuation of the spectra shown in the two frames on the

---

[1] The products of the neutral pions generated at the IP and immediately decaying are considered instead of the parent particle.

right of FIG. 3., particularly enhanced for the Q1, because of the thicker BS (see section 3.1). Protons are captured in a smaller amount, but in particular in the Q3. The spectra of the neutral particles clearly show the purely geometrical shadowing effect provided by the TAS, protecting the first two elements of the triplet. Secondary particles generated by the debris impacting on beam line elements (e.g. the TAS) are responsible for the tails in the energy region below 100 GeV. Spectra reaching the downstream elements (e.g. the corrector package) are represented by the purple lines.
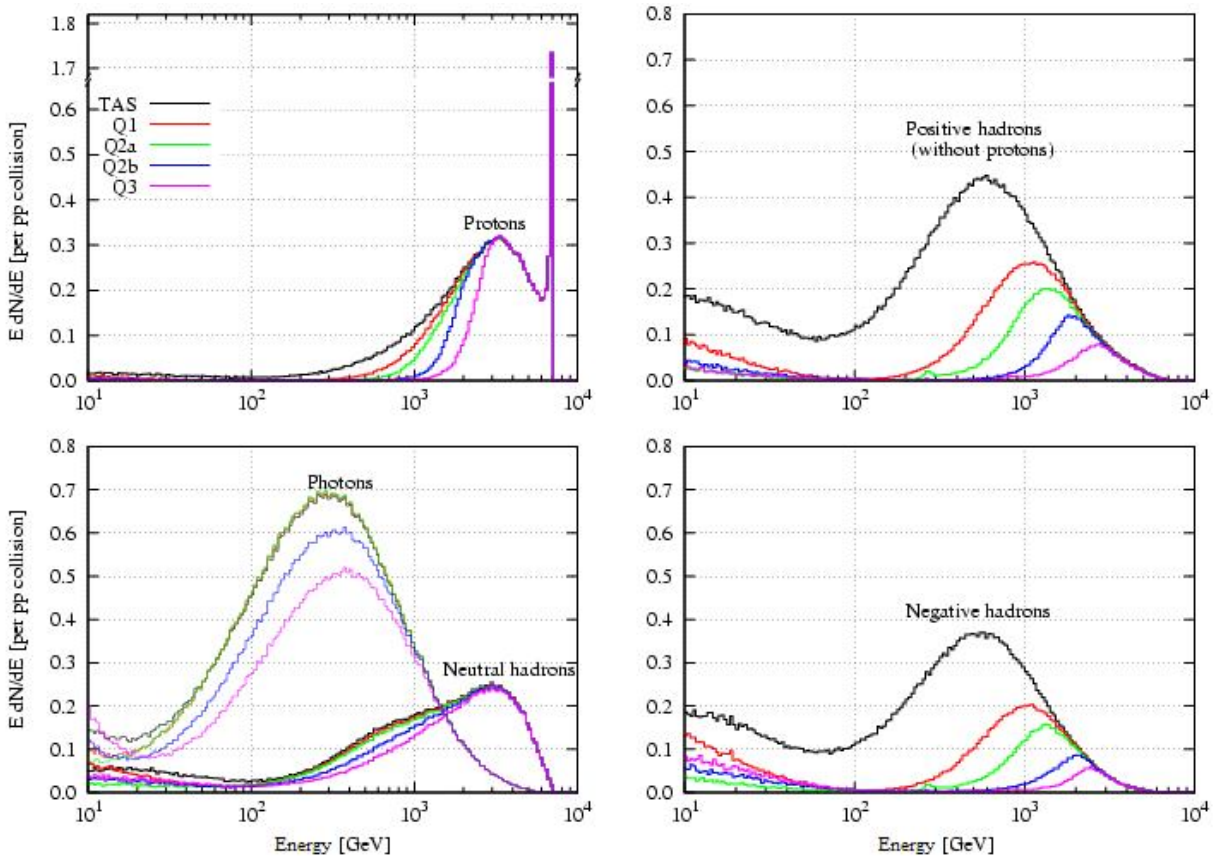

FIG. 3. Particle spectra in the vacuum chamber at the non-IP side of the TAS and of each triplet element. The four frames refer to the most relevant particle families.

3. Protecting the triplet

A previous study [8] on the Phase I Upgrade showed the dependence of the power deposition in the triplet on the triplet length[2]: for the luminosity of 2.5 L_0 the design limit is respected all along the triplet length but at the non-IP side of the Q1 and at the IP side of the Q2a (the first module of the Q2).

A continuous liner (e.g. 3 mm of Tungsten) inside the vacuum chamber can effectively lower the values of power deposition in the most critical location. Its extension in the interconnections is important in order not to have a larger aperture over the longitudinal separation between magnets causing a pronounced peak at the IP side of the downstream element. Another option would be to

---

[2] Magnetic field gradients and magnet aperture scale consequently.

locally shield the IP side of the Q2a with thick end plates outside the Cold Bore Tube (CBT), but this is of quite limited help because of the main shower coming from the inside.

3.1.   A thick liner in the Q1 and the geometrical shadowing effect

Since the beam size in the Q1 is smaller than in the rest of the triplet, the larger clearance between the beam envelope and the magnet aperture allows to lodge a thick liner, welded to the BS, shielding not only the magnet itself but also the first part of the downstream Q2a, where the highest peak power is located. The net benefit is clearly visible in FIG. 4. (there and in the following the power values refer to 2.5 L_0): the longitudinal pattern of the peak power density in the triplet coils for a previous Phase I Upgrade triplet design (featuring an aperture of 130 mm and one corrector magnet between the Q1 and the Q2a) changes in the Q1, in the downstream corrector and in the Q2a (IP side) if the extra-thickness of the BS is increased from 8 mm (black curve) to 13 mm (blue curve). Not only the peak power in the first half of the triplet is decreased, but also a fraction of the heat load is moved from the cryogenic system of the magnet onto the cryogenic system of the BS, working at a higher temperature. The preferred 120 mm coil aperture design shown in FIG. 2 implements a 10 mm thick stainless steel liner in the Q1 in addition to a 2 mm thick BS and a 3.2 mm thick CBT all along the triplet.
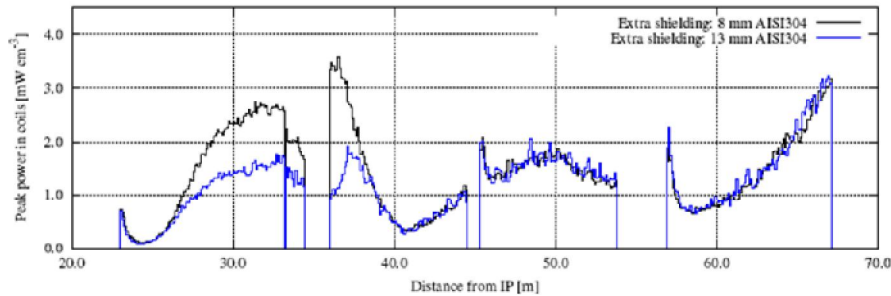

FIG. 4. Peak power density in the triplet cables for different thicknesses of the additional shield inside the Q1. The study refers to a previous Phase I Upgrade triplet design.

3.2.   Crossing scheme and triplet magnetic configuration

In the LHC operation, the proton-proton collisions will be featured by a crossing angle lying on the horizontal or vertical plane and symmetric with respect to the longitudinal axis. The magnetic configuration of the triplet for a positive charged particle escaping the IP is FDDF with respect to the *horizontal* plane, whereas it has the opposite sign, i.e. DFFD, with respect to the *vertical* plane. Thus, the coupling of the crossing scheme with the magnetic configuration of the triplet sets the shape of the energy deposition pattern and in particular the location of the peaks inside the superconducting coils.

FIG. 5. shows the longitudinal profile of the peak power density for both vertical and horizontal crossing scheme for the 120 mm coil aperture triplet design; an intermediate case with the crossing plane at 45º (for which the outgoing beam is directed towards the positive *x* and *y*) is also shown; transverse maps of power deposition superimposed to the magnet sections are also given at the longitudinal maxima indicated by the arrows. For *vertical* crossing the peaks are clearly located on the crossing plane, at the IP side of the Q2a (an element defocusing on the crossing plane) and at the end of the Q3 (vertically defocusing). For *horizontal* crossing, on the

contrary, the peak on the IP side of the Q2a is lower (after an element focusing on the crossing plane) and a peak at the IP side of the Q3 clearly arises (after two horizontally defocusing modules, the second of which is already quite loaded). A common feature of the two different crossing schemes is the reversal of the peak position: e.g., for *horizontal* crossing, the peak is moved in the magnet cross section from the initial position at right ($x>0$, where the half crossing angle points) to left ($x<0$), as can be seen from the two central maps in the bottom frames of FIG. 5. For *vertical* crossing, it moves from the top to the bottom (see the first and last maps). Moreover, the opposite behavior of the peak profile in the Q3 anticipates the different impact of the debris on the following corrector package (see Section 4).
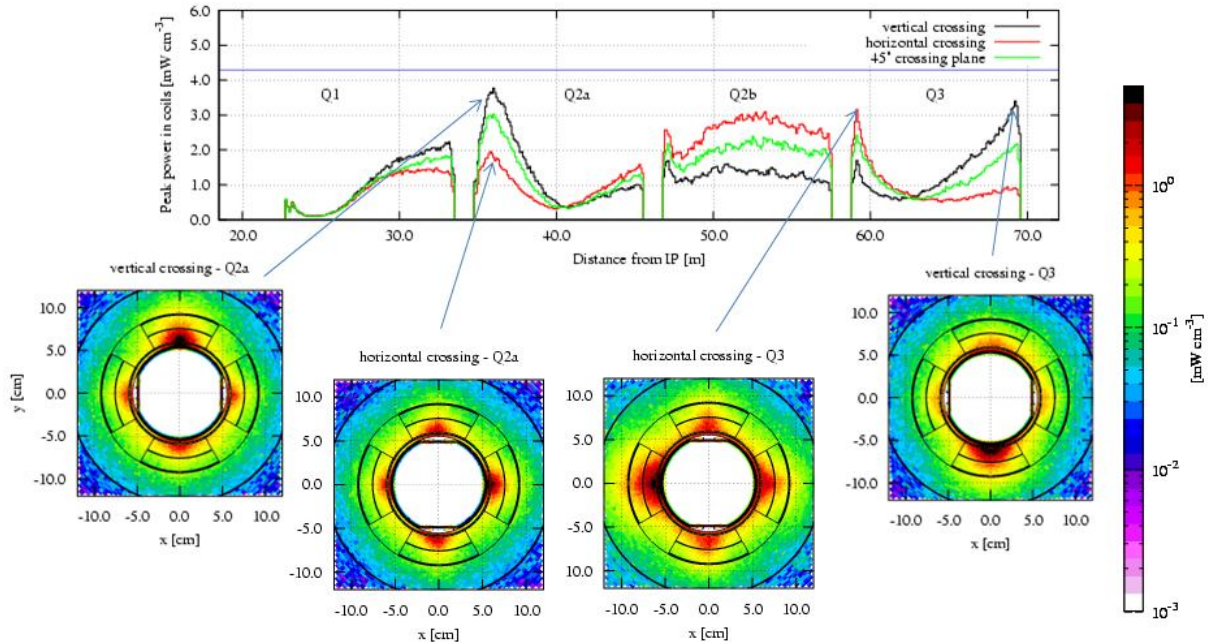

FIG. 5. Top frame: longitudinal profile of the peak power density in the triplet superconducting cables for vertical (black) and horizontal (red) crossing scheme. A case with the crossing plane at 45° is also shown (green curve). Bottom frame: cross sectional maps of power deposition in the magnets at the longitudinal maxima indicated by the arrows.

The case referring to the 45° crossing scheme (green curve in FIG. 5.) is in-between the other two: it gathers the features of both, but quantitatively attenuated. See for instance the two peaks appearing in the Q3, the first one located on the horizontal plane at the left (as for horizontal crossing) and the second one on the vertical plane downside (as for vertical crossing).

4. Protecting the corrector package

The proposed Phase I Upgrade design of the corrector package [2] is composed by a short sextupole followed by a skew quadrupole, and two dipoles, the first one acting on the horizontal plane and the second one acting on the vertical plane (see FIG. 6.). The coil geometry was accurately implemented in FLUKA for all the elements but not for the sextupole, for which a ring with the right aperture was used. A more realistic implementation of this element is under development.

FIG. 7. shows the longitudinal profile of the peak power density in the corrector package in case of *vertical* crossing, for different apertures of the corrector package itself. The red curve refers to the 120 mm aperture case, the same aperture as in the triplet, whereas the black curve refers to the 140 mm aperture case. The **aperture increase** from the triplet to the corrector package brings the latter under the shadow originated by the former, with a clear benefit particularly enhanced on the sextupole. The two central elements (the skew quadrupole and the horizontal corrector) show values quite low and similar for both apertures, since they profit from the favourable **coil position**, not located on the vertical axis (where the peak is expected to lie for vertical crossing). The 140 mm aperture case was also studied with a Copper liner inside the coil aperture all along the corrector package elements (blue curve in FIG. 7.): peak power density values significantly decrease, with the exception of the IP side of the sextupole, which would have had benefits only if extending the shielding upstream.

In case of *horizontal* crossing the focalization in the Q3 (see FIG. 5.) reduces the debris capture in the corrector package, lowering peak values: the pattern is almost constant around 1 mW·cm^{-3}.
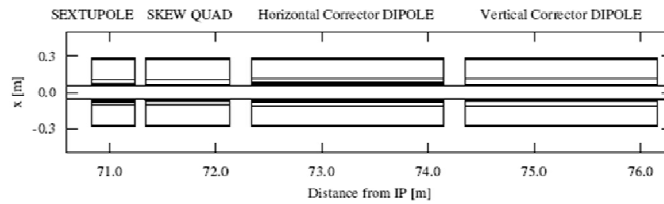

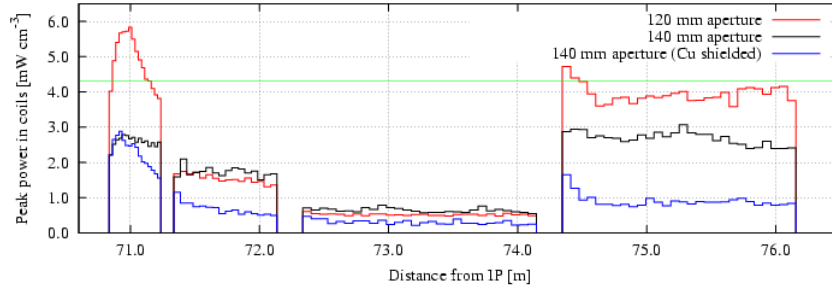FIG. 6. *Layout of the corrector package for the Phase I Upgrade: FLUKA implementation.*

FIG. 7. *Longitudinal profile of peak power density in the corrector package for vertical crossing. Two different apertures are considered: 120 mm (as in the triplet, red curve) and 140 mm (black curve). The blue curve refers to the 140 mm aperture case with a 10 mm thick copper liner inside the magnet aperture.*

5. The first separation dipole

Adopting the 180 mm aperture D1 mentioned in Section 1, peak power values in its coils are below 1 mW·cm^{-3}, not representing a worry as far as the risk of quench is concerned.

6. Total heat load

A global view of the power deposition over the new insertion region is given for *vertical* crossing in FIG. 8.: the cut is on the vertical plane and the black areas exceed 5 mW·cm^{-3}. It should be noted that the resolution of the map is finer than the scoring bin size used to evaluate the peak power deposition relevant to quench risk calculations, which is actually averaged over a

minimum thermal equilibrium volume, taking the width/height of the scoring bin equal to the superconducting cable transverse dimensions and the length equal to the cable twist pitch. The reversal of the debris impact point can be appreciated looking at the Q2a IP side (where the maximum is found at $y>0$) and at the triplet end and downstream (where the maximum is found at $y<0$).

TABLE I lists the values of the total load on the different elements. The contribution of the BS is kept separated from the total on the respective element. The horizontal crossing scheme turns out to be slightly preferable, because less debris is captured by the magnetic fields. Thus, the impact on further downstream elements has to be investigated.
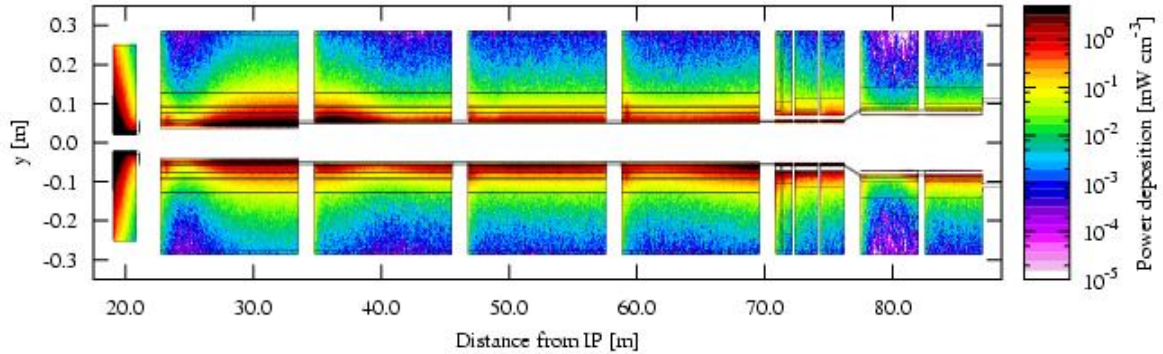

FIG. 8. Global view of the power deposition in the TAS-D1 region for vertical crossing. The TAS, the four modules of the triplet, the four elements of the corrector package and the two modules of the first separation dipole are shown. The cut is on the vertical plane. Black areas exceed 5 mW·cm^{-3}.

7. Conclusions

The magnetic field plays an important role in capturing the charged component of the debris (especially high energy pions), leading it to shower outside the BS and to induce power deposition in the superconducting cables, with possible risk of quench.

The TAS effectively reduces the load onto the Q1. Hot spots are expected to be found at the non-IP side of the Q1 and at the IP side of the Q2a. Peaks lie on the crossing plane and change their position (from top to bottom, from left to right) in the Q2a. A continuous liner inside the aperture and extended along the interconnections provides the superconducting cables with substantial shield. A thicker BS in the Q1 is effective up to the first half of the Q2a.

The vertical crossing scheme is more harmful for the downstream elements of the IR beam line. Nevertheless the azimuthal position of the coils with respect to the crossing plane can be critical (e.g., the favourable position of the poles of the horizontal corrector dipole). Increasing the aperture with respect to the upstream elements generates an effective shadowing, in particular on the first element of the downstream magnet string. A 10 mm thick Copper liner can be of help.

Due to the very large aperture of 180 mm, the D1 does not represent an issue.

TABLE I: TOTAL VALUES OF POWER DEPOSITION ON EACH BEAM LINE ELEMENT (BS EXCLUDED), AND LOAD ON THE RESPECTIVE BS. VALUES ARE ALSO GIVEN FOR EACH FUNCTIONAL GROUP OF ELEMENTS. TOTALS MAY NOT CORRESPOND TO THE SUM DUE TO ROUNDING. VALUES ARE GIVEN IN W.

		vertical crossing		*horizontal crossing*	
		element	*BS*	*element*	*BS*
TAS		**384**	**-**	**382**	**-**
triplet	TOT	**341**	**95**	**332**	**93**
	Q1	84	60	82	59
	Q2a	68	8	64	7
	Q2b	94	13	103	14
	Q3	95	15	82	13
corr. package	TOT	**50**	**11**	**33**	**8**
	sextupole	7	1	5	1
	skew quad	9	2	6	1
	hor. dipole	17	4	13	3
	vert. dipole	17	4	11	3
D1	TOT	**33**	**5**	**23**	**3**
	first module	12	1	10	1
	second module	21	3	13	3
Total load		**808**	**111**	**770**	**105**

References
[1]   EUROPEAN ORGANIZATION FOR NUCLEAR RESEARCH, LHC Design Report, CERN-2004-003, Geneva (2004).
[2]   http://slhc-irp1.web.cern.ch/SLHC-IRP1/
[3]   MOKHOV, N.V., et al., Protecting LHC IP1/IP5 Components against Radiation Resulting from Colliding Beam Interactions, LHC Project Report 633, Geneva (2003).
[4]   BAGLIN, V., et al., Conceptual Design of the LHC Interaction Region Upgrade – Phase-I, LHC Project Report 1163, Geneva (2008).
[5]   FERRARI, A., et al., FLUKA: a Multi-Particle Transport Code, CERN-2005-10 (2005), INFN/TC_05/11, SLAC-R-773.
[6]   BATTISTONI, G., et al., The FLUKA Code: Description and Benchmarking, Proceedings of the Hadronic Shower Simulation Workshop 2006, Fermilab 6-8 September 2006, M. Albrow, R.Raja eds., AIP Conference Proceeding 896 (2007) 31-49
[7]   ROESLER, S., et al., The Monte Carlo Event Generator DPMJET-III, Proceedings of the Monte Carlo 2000 Conference, Lisbon, October 23-26 2000, A. Kling, F. Barao, M. Nakagawa, L. Tavora, P. Vaz eds., Springer-Verlag Berlin (2001) 1033-1038.
[8]   WILDNER, E., et al., Parametric Study of Energy Deposition in the LHC Inner Triplet for the Phase I Upgrade, LHC Project Report 1127, Geneva (2008).